Simultaneous Localization and Planning for Cooperative Air Munitions

Andrew J. Sinclair[1], Richard J. Prazenica[2], and David E. Jeffcoat[3]

[1] Auburn University, Auburn AL 36849, USA
[2] University of Florida, Shalimar FL 32579, USA
[3] Air Force Research Laboratory, Eglin Air Force Base FL, USA

Abstract. This chapter considers the cooperative control of aerial munitions during the attack phase of a mission against ground targets. It is assumed that sensor information from multiple munitions is available to refine an estimate of the target location. Based on models of the munition dynamics and sensor performance, munition trajectories are designed that enhance the ability to cooperatively estimate the target location. The problem is posed as an optimal control problem using a cost function based on the variances in the target-location estimate. These variances are computed by fusing the individual munition measurements in a weighted least squares estimate. Numerical solutions are found for several examples both with and without considering limitations on the munitions' field of view. These examples show large reductions in target-location uncertainty when these trajectories are used compared to other naively designed trajectories. This reduction in uncertainty could enable the attack of targets with greater precision using smaller, cheaper munitions.

1 Introduction

Research is in progress on the cooperative control of air armament designed to detect, identify, and attack ground targets. One class of this type of armament are wide-area search munitions, which can be deployed in an area of unknown targets. Current development is focused on possibilities of enhancing munition capabilities through cooperative control. This chapter presents a new concept for developing trajectories that enhance munitions' capability to cooperatively estimate target locations.

The tasks of intercepting a chosen target and estimating the target's location can represent competing requirements in the path planning of a munition. In a general sense, the problem posed here is to plan a path to a target while simultaneously estimating that target's location. This can be considered a simultaneous localization and planning (SLAP) problem. Whereas SLAP problems can be studied for a single agent, many interesting behaviors emerge when cooperative agents are considered.

Important work exists in the literature on the two related problems of cooperative search [1,2,3] and the design of optimal trajectories for single observers

M.J. Hirsch et al. (Eds.): Adv. in Cooper. Ctrl. & Optimization, LNCIS 369, pp. 81–93, 2007.
springerlink.com

[4,5,6,7,8,9,10]. Much of the work in optimal trajectories has focused on bearings-only measurements of a target, often focused on sonar applications. Fawcett investigated the impact of maneuvers on the Cramer-Rao lower bound for the target-state estimate [4]. Frew and Rock investigated a method to minimize a measure of the estimate error covariance [9]. Other works have studied optimal trajectories for cooperative observers [11,12]. These works have focused on reconnaissance of a target, relating the performance index to the quality of the target-location estimate at the end of the mission or a time interval.

Several related topics also capture aspects of both cooperative search and trajectory design. Dohner et al. used a Lyapunov approach to drive a vehicle swarm to an uncertain target location while simultaneously maintaining swarm spacing to ensure observability of the target [13]. Passino et al. developed a distributed cooperative search algorithm where decisions were made planning into the future to minimize a cost function representing several subgoals, such as covering areas in large uncertainty and minimizing overlap with other agents [14].

It is noteworthy that the problem considered in this chapter, trajectory design to enhance target-location estimation, is in some ways the dual of another problem that has received considerable attention, trajectory design to minimize detection by an enemy radar [15,16,17,18]. Pachter et al. have considered another related problem that used cooperative vehicles to project phantom tracks to an enemy radar [19,20].

This chapter extends the field of optimal observor trajectories to the cooperative-attack application. The methods presented in this chapter will be illustrated for a planar problem with two munitions and one target; the methods apply though to three-dimensional cases with general numbers of munitions and targets. In the following section, models for the munition motion and sensor performance are presented. Next, the SLAP trajectory design is posed as an optimal control problem. Several example numerical solutions are then presented. Finally, the performance of a target-location estimation algorithm is evaluated along the SLAP trajectories and compared to alternative trajectories.

2 Model Development

A scenario can be considered with the two-dimensional plane populated by n munitions and m fixed targets. The following developments will illustrate the method for two munitions and one target. The state of each munition is given by its position in two dimensional space, $\boldsymbol{x}_1 = [x_1 \; y_1]^\mathsf{T}$ and $\boldsymbol{x}_2 = [x_2 \; y_2]^\mathsf{T}$. A constant-speed kinematic model is used to describe the motion of the munitions. The heading angles of the munitions are ψ_1 and ψ_2, and the speed of each munition is v.

$$\begin{aligned} \dot{x}_1 &= v\cos\psi_1 \quad ; \quad \dot{x}_2 = v\cos\psi_2 \\ \dot{y}_1 &= v\sin\psi_1 \quad ; \quad \dot{y}_2 = v\sin\psi_2 \end{aligned} \tag{1}$$

$$\dot{\boldsymbol{x}}_i = \boldsymbol{f}_i\left(\psi_i\right), \quad i \in \{1,2\} \tag{2}$$

Here, the heading angles are treated as control variables.

Additionally, each munition is considered to carry a sensor that is capable of measuring the target location in the xy plane. Again, the end goal will be to design trajectories that improve the estimation of the target location. Therefore, a model is needed of the sensor measurements and their uncertainties. The target has a position described by $\boldsymbol{x}_T = [x_T \; y_T]^\mathsf{T}$. The measurement of this target location by each munition, $\tilde{\boldsymbol{z}}_1 = [\tilde{x}_{T,1} \; \tilde{y}_{T,1}]^\mathsf{T}$ and $\tilde{\boldsymbol{z}}_2 = [\tilde{x}_{T,2} \; \tilde{y}_{T,2}]^\mathsf{T}$, is modeled as shown below.

$$\begin{aligned} \tilde{x}_{T,1} &= x_T + w_{x,1}(0, \sigma_{x,1}) \quad ; \quad \tilde{x}_{T,2} = x_T + w_{x,2}(0, \sigma_{x,2}) \\ \tilde{y}_{T,1} &= y_T + w_{y,1}(0, \sigma_{y,1}) \quad ; \quad \tilde{y}_{T,2} = y_T + w_{y,2}(0, \sigma_{y,2}) \end{aligned} \tag{3}$$

The measurement errors from each munition are assumed to be independent of the errors from the other munition. The x and y measurement errors from each individual munition, however, are treated as correlated Gaussian random variables with zero mean and standard deviations of $\sigma_{x,i}$ and $\sigma_{y,i}$, where $i \in \{1, 2\}$. It is these uncertainties that will drive the trajectory design, and they can be selected to model a particular sensor design.

The error in the target-location measurements from an individual munition is treated as following a zero-mean jointly-Gaussian distribution that is uncorrelated in the down-range and cross-range directions, relative to the true target and munition locations. The errors in these directions, $w_{d,i}(0, \sigma_{d,i})$ and $w_{c,i}(0, \sigma_{c,i})$, can therefore be treated as independent Gaussian random variables. The standard deviations in the down-range and cross-range directions are modeled as functions of the range from the munition to the target.

$$\sigma_{d,i} = 0.1 r_i \quad ; \quad \sigma_{c,i} = 0.01 r_i \tag{4}$$

This models a sensor that is more accurate when close to the target and more accurate in the transverse direction than in the radial direction. The uncertainty in the measurement of the target location by the ith munition is illustrated in Fig. 1.

From the down-range and cross-range variables, the errors and the covariance matrix in the x and y coordinates can be found.

$$\begin{bmatrix} w_{x,i} \\ w_{y,i} \end{bmatrix} = \begin{bmatrix} \cos\theta_i & \sin\theta_i \\ -\sin\theta_i & \cos\theta_i \end{bmatrix} \begin{bmatrix} w_{d,i} \\ w_{c,i} \end{bmatrix} \tag{5}$$

$$\boldsymbol{P}_i = \begin{bmatrix} \sigma_{x,i}^2 & \sigma_{xy,i} \\ \sigma_{xy,i} & \sigma_{y,i}^2 \end{bmatrix} = \begin{bmatrix} \cos\theta_i & \sin\theta_i \\ -\sin\theta_i & \cos\theta_i \end{bmatrix} \begin{bmatrix} \sigma_{d,i}^2 & 0 \\ 0 & \sigma_{c,i}^2 \end{bmatrix} \begin{bmatrix} \cos\theta_i & -\sin\theta_i \\ \sin\theta_i & \cos\theta_i \end{bmatrix} \tag{6}$$

Here, θ_i is the bearing angle of the target relative to the ith munition. The range and bearing angle for each target-munition pair are computed as shown below.

$$r_i = \sqrt{(x_T - x_i)^2 + (y_T - y_i)^2} \tag{7}$$

$$\theta_i = \tan^{-1}\left(\frac{y_T - y_i}{x_T - x_i}\right) \tag{8}$$

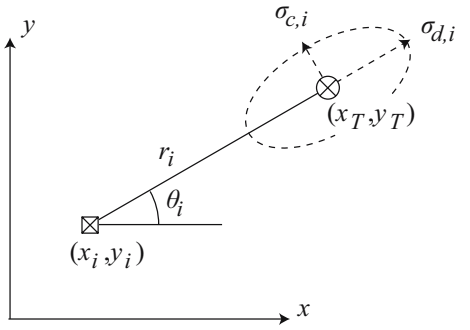

Fig. 1. Measurement of the target by the ith munition and the associated error probability ellipse

The significance of Eq. (6) is that it models the quality of the measurements from the ith munition based on its position relative to the target.

The measurements provided by both munitions can be fused into a single instantaneous estimate of the target location. This is done using a weighted least-squares estimator (WLSE) [21,22]. The measurements of the target location from each munition are grouped into a measurement vector $\tilde{\boldsymbol{z}} = [\tilde{x}_{T,1}\ \tilde{y}_{T,1}\ \tilde{x}_{T,2}\ \tilde{y}_{T,2}]^\mathsf{T}$. This produces a linear measurement model in terms of the target location.

$$\boldsymbol{z} = \boldsymbol{H}\boldsymbol{x}_T + \boldsymbol{w} \tag{9}$$

$$\boldsymbol{H} = \begin{bmatrix} 1\,0\,1\,0 \\ 0\,1\,0\,1 \end{bmatrix}^\mathsf{T}; \qquad \boldsymbol{w} = \begin{bmatrix} w_{x,1}\ w_{y,1}\ w_{x,2}\ w_{y,2} \end{bmatrix}^\mathsf{T} \tag{10}$$

Here, $\boldsymbol{w}$ is the vector of measurement errors. The covariance of this error vector is given by arranging the covariances from each munition.

$$\boldsymbol{R} = \begin{bmatrix} \boldsymbol{P}_1 & \boldsymbol{0} \\ \boldsymbol{0} & \boldsymbol{P}_2 \end{bmatrix} \tag{11}$$

The instantaneous WLSE of the ith target location and the associated covariance are given by the following.

$$\hat{\boldsymbol{x}}_T = \left(\boldsymbol{H}^\mathsf{T}\boldsymbol{R}^{-1}\boldsymbol{H}\right)^{-1}\boldsymbol{H}^\mathsf{T}\boldsymbol{R}^{-1}\tilde{\boldsymbol{z}} \tag{12}$$

$$\boldsymbol{P} = \left(\boldsymbol{H}^\mathsf{T}\boldsymbol{R}^{-1}\boldsymbol{H}\right)^{-1} \tag{13}$$

Considering the first of Eqs. (10), the WLSE reduces to the following.

$$\hat{\boldsymbol{x}}_T = \begin{bmatrix} \hat{x}_T \\ \hat{y}_T \end{bmatrix} = \left(\boldsymbol{P}_1^{-1} + \boldsymbol{P}_2^{-1}\right)^{-1}\left(\boldsymbol{P}_1^{-1}\tilde{\boldsymbol{z}}_1 + \boldsymbol{P}_2^{-1}\tilde{\boldsymbol{z}}_2\right) \tag{14}$$

More importantly for the current purposes, the covariance of this combined estimate is related to the individual covariances of the measurements from each munition.

$$\boldsymbol{P} = \begin{bmatrix} \sigma_x^2 & \sigma_{xy} \\ \sigma_{xy} & \sigma_y^2 \end{bmatrix} = \left(\boldsymbol{P}_1^{-1} + \boldsymbol{P}_2^{-1}\right)^{-1} \tag{15}$$

The covariance $\boldsymbol{P}$ now models the quality of the combined target-location estimate based on the positioning of the two munitions relative to the target. For cases with more than two munitions, similar expressions can be developed combining the measurements of each of the munitions. Additionally, for cases with multiple targets corresponding expressions can be used for the covariance of each target-location estimate.

3 Problem Formulation

The task of designing trajectories for the munitions in order to enhance the estimation performance can now be posed as the following optimal control problem. Consider the state vector $\boldsymbol{x} = [x_1\ y_1\ x_2\ y_2]^\mathsf{T}$. The heading angles of the munitions can be organized into a control vector $\boldsymbol{u} = [\psi_1\ \psi_2]^\mathsf{T}$. The state vector evolves according to the state equation found by grouping Eq. (2), $\dot{\boldsymbol{x}} = \boldsymbol{f}(\boldsymbol{u}) = [\boldsymbol{f}_1^\mathsf{T}\ \boldsymbol{f}_2^\mathsf{T}]^\mathsf{T}$. For boundary conditions, the initial positions of the munitions will be considered a given, and the final position of munition 1 is required to be the target location, $x_1(t_F) = x_T$ and $y_1(t_F) = y_T$. The final position of munition 2 is free.

The goal will be to find the trajectories that minimize the following cost function, which is based on the WLSE covariance.

$$J = \int_0^{t_F} \left(\sigma_x^2 + \sigma_y^2\right) \mathrm{d}t \tag{16}$$

The variances of each target location are functions of the states describing the munition configuration. Clearly, this cost function emphasizes the uncertainty over the entire trajectory. Previous works have used performance indices related to the uncertainty at the end of the trajectory or a specified interval [11,12]. Compared to those alternative indices, the cost function used here encourages reduction in uncertainty earlier in the trajectory. It is also noted that other cost functions could be based on the determinant or other metrics of the covariance matrix.

Introducing the costates $\boldsymbol{\lambda}(t) = [\lambda_1\ \lambda_2\ \lambda_3\ \lambda_4]^\mathsf{T}$, a time-varying vector of Lagrange multipliers, the Hamiltonian can be defined.

$$H = \sigma_x^2 + \sigma_y^2 + \boldsymbol{\lambda}^\mathsf{T} \boldsymbol{f}(\boldsymbol{u}) \tag{17}$$

From this, the first-order necessary conditions are derived [23].

$$\frac{\partial H}{\partial \boldsymbol{u}} = \left(\frac{\partial \boldsymbol{f}}{\partial \boldsymbol{u}}\right)^\mathsf{T} \boldsymbol{\lambda} = \boldsymbol{0} \tag{18}$$

$$\dot{\boldsymbol{\lambda}} = -\frac{\partial H}{\partial \boldsymbol{x}} = -\frac{\partial}{\partial \boldsymbol{x}} \left(\sigma_x^2 + \sigma_y^2\right) \tag{19}$$

From Eq. (18) the control law for the heading angles as a function of the costates can be found.

$$\frac{\partial H}{\partial \psi_1} = -\lambda_1 v \sin\psi_1 + \lambda_2 v \cos\psi_1 = 0 \tag{20}$$

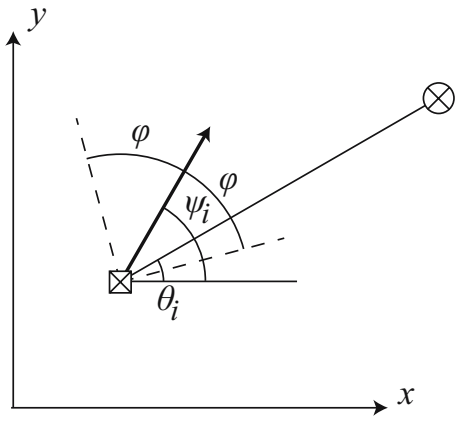

Fig. 2. Heading angle, field-of-view half angle, bearing angle of ith munition relative to the target

$$\frac{\partial H}{\partial \psi_2} = -\lambda_3 v \sin\psi_2 + \lambda_4 v \cos\psi_2 = 0 \tag{21}$$

To find a minimum in the cost, the following curvature condition is additionally imposed.

$$\frac{\partial^2 H}{\partial \psi_1^2} = -\lambda_1 v \cos\psi_1 - \lambda_2 v \sin\psi_1 > 0 \tag{22}$$

$$\frac{\partial^2 H}{\partial \psi_2^2} = -\lambda_3 v \cos\psi_2 - \lambda_4 v \sin\psi_2 > 0 \tag{23}$$

This gives the optimal control as the following.

$$\psi_1 = \tan^{-1}\left(\frac{-\lambda_2}{-\lambda_1}\right) \quad ; \quad \psi_2 = \tan^{-1}\left(\frac{-\lambda_3}{-\lambda_4}\right) \tag{24}$$

The costate equations, governing the evolution of $\boldsymbol{\lambda}$ are given by Eq. (19). These can be found by applying the chain rule to Eqs. (4), (6-8), and (15); however, they are rather extended and are not reproduced here. The terminal conditions for the problem are the specified conditions, $x_1(t_F) = x_T$ and $y_1(t_F) = y_T$, and the necessary conditions, $\lambda_3(t_F) = \lambda_4(t_F) = H(t_F) = 0$.

The above conditions have not accounted for limitations in the field of view of the vehicle sensors. This assumes either a sensor that has unlimited field of view or is gimbal mounted in order to view a target regardless of the vehicle orientation and heading. A sensor that is fixed mounted on the vehicle, though, may only offer a limited field of view relative to the vehicle heading. In this case a hard constraint can be enforced on the trajectory of the ith munition to keep the target in view. The field of view angle is labeled 2ϕ and is illustrated in Fig. 2.

Two inequality constraint functions can be enforced to keep the target in the field of view of the ith munition. For example, the following constraints keep the target in the field of view of munition 1.

$$c_1 = \psi_1 - \theta_1 - \phi \leq 0 \qquad ; \qquad c_2 = -\psi_1 + \theta_1 - \phi \leq 0 \tag{25}$$

Note that the bearing angles are functions of the states, and the heading angles are the controls. Arranging any desired constraints into a vector function $\boldsymbol{c}(\boldsymbol{x}, \boldsymbol{u}) \leq \boldsymbol{0}$ and introducing a second set of Lagrange multipliers $\boldsymbol{\mu}$, a revised Hamiltonian is developed [23].

$$H = \sigma_x^2 + \sigma_y^2 + \boldsymbol{\lambda}^\mathsf{T} \boldsymbol{f}(\boldsymbol{u}) + \boldsymbol{\mu}^\mathsf{T} \boldsymbol{c}(\boldsymbol{x}, \boldsymbol{u}) \tag{26}$$

During periods when one or more of these constraints are active, the target is kept on the edge of the field of view of the munition. The value of $\boldsymbol{\mu}$ is calculated from the revised stationary condition.

$$\begin{aligned} \frac{\partial H}{\partial \psi_1} &= -\lambda_1 v \sin\psi_1 + \lambda_2 v \cos\psi_1 + \boldsymbol{\mu}^\mathsf{T} \tfrac{\partial \boldsymbol{c}}{\partial \psi_1} = 0 \\ \frac{\partial H}{\partial \psi_2} &= -\lambda_3 v \sin\psi_2 + \lambda_4 v \cos\psi_2 + \boldsymbol{\mu}^\mathsf{T} \tfrac{\partial \boldsymbol{c}}{\partial \psi_2} = 0 \end{aligned} \tag{27}$$

The costate equations are revised as shown below.

$$\dot{\boldsymbol{\lambda}} = -\frac{\partial H}{\partial \boldsymbol{x}} = -\frac{\partial}{\partial \boldsymbol{x}} \left(\sigma_x^2 + \sigma_y^2\right) + \left(\frac{\partial \boldsymbol{c}}{\partial \boldsymbol{x}}\right)^\mathsf{T} \boldsymbol{\mu} \tag{28}$$

The two-point boundary-value problem can now be posed to solve for $\boldsymbol{\lambda}(t_0)$ and t_F subject to the derived necessary conditions and the boundary conditions. When the field-of-view constraints are inactive or simply neglected, the necessary conditions are Eqs. (2), (19), and (24). When the field-of-view constraint is active, the necessary conditions are Eqs. (2), (27), and (28).

For cases with more than two munitions or more than one target, the terminal conditions could be specified by prechosen target-munition attack pairings. The final states for any munitions not assigned a target would be free. For multiple targets, the cost function could be augmented by summing the additional variances from their target-location estimates. For complex scenarios with many targets and munitions, difficulty may arise in the application of the field-of-view constraints. It may be desirable to let targets pass in and out of the field of view of some munitions.

For any scenario, the solution of the problem produces munition trajectories designed to reduce the uncertainty in the target-location estimates. These are referred to as the SLAP trajectories. Note that in a real-time application, the use of the true target positions as boundary conditions would not be possible. These must be estimated, which is the motivation behind finding the SLAP trajectories in the first place. Here, though, the true locations are used to illustrate the concept and potential benefit of these trajectories.

4 Sample SLAP Trajectories

The following are several example SLAP trajectories that have been found using a sequential quadratic programming algorithm to numerically search for the optimization parameters. Each of the examples considers the scenario of two munitions and one target. Munition 1 is assigned to attack the target, and munition 2 is free to assist in the estimation of the target location. Two different initial conditions are considered, and solutions are presented with and without the field-of-view constraint. Here, a munition speed of $v = 300\,\text{ft/sec}$ and a half field-of-view angle of $\phi = 45\,\text{deg}$ were used.

The first set of initial conditions are $x_1(0) = 0\,\text{ft}$, $y_1(0) = -2000\,\text{ft}$, $x_2(0) = 100\,\text{ft}$, and $y_2(0) = -2000\,\text{ft}$. The target is located at $x_T = y_T = 0\,\text{ft}$. This problem was first solved neglecting any field-of-view constraints. The solution parameters found for this case are shown in Table 1 under problem 1.

Table 1. Solution parameters and cost for sample SLAP trajectories

solution parameters	problem 1	problem 2	problem 3	problem 4
$\lambda_1(0)$	29.495	32.226	30.550	32.453
$\lambda_2(0)$	−12.028	−12.745	−14.236	−15.170
$\lambda_3(0)$	−28.822	−49.167	30.551	49.532
$\lambda_4(0)$	−13.460	−40.658	14.258	40.001
t_F (sec)	8.0950	7.6325	8.2146	7.6769
J	1.59×10^4	1.70×10^4	1.89×10^4	2.02×10^4

The trajectories generated by these values are shown in Fig. 3(a). The marks along the trajectories in the figure indicate one-second intervals of flight time. In this case the SLAP trajectories are roughly symmetric about the y axis. Munition 1 intercepts the target at t_F as required by the boundary conditions, but munition 2 also approaches the target very closely. Intuitively this is because the measurement errors from either munition are reduced as the munition closes the range with the target. Instead of traveling directly to the target, however, near the initial time both munitions sweep out in the $\pm x$ directions. This gives the munitions differing perspectives on the target allowing them to compensate for the relatively large downrange errors in each other's measurements.

In the trajectories for problem 1, both munitions sweep out aggressively such that the target would be out of their fields of view during the initial stages of the trajectories. To correct for this, problem 2 is posed to enforce that both munitions keep the target within view. Problem 2 is identical to problem 1 in all other aspects. The solutions for this problem are shown in Table 1 and the corresponding trajectories are shown in Fig. 3(b).

In this case, the field-of-view constraint is active over the entire trajectory of munition 2. It is prevented from swinging wide during the initial periods, and instead munition 2 keeps the target on the edge of its field of view for the entire flight. The field-of-view constraint is also initially active for munition 1.

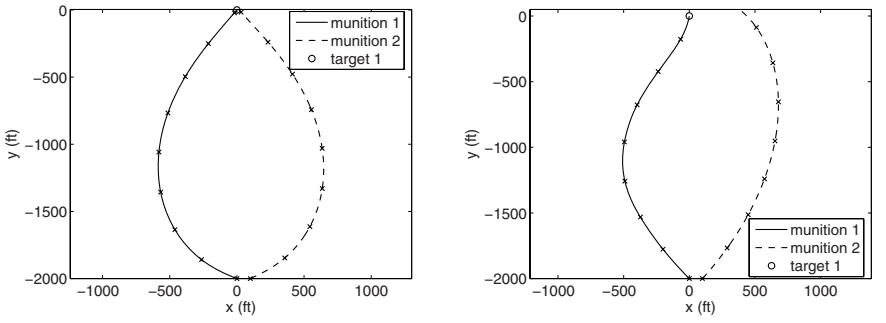

Fig. 3. SLAP trajectories for problems 1 and 2

After a short period, though, munition 1 turns to head more directly toward the target. Again, the intuitive behaviors of closing range to the target and achieving differing points of view are present in the SLAP trajectories for problem 2. The motions are restricted, however, by the field-of-view constraint.

Next, a different initial condition can be considered with munition 2 moved to an initial position $x_2(0) = 0\,\text{ft}$, and $y_2(0) = 2000\,\text{ft}$. Instead of starting nearby munition 1, munition 2 now starts on the opposite side of the target relative to munition 1. The solution for this case when neglecting the field-of-view constraint is shown as problem 3 in Table 1. The SLAP trajectories for this problem are shown in Fig. 4(a). The trajectories for the two munitions are nearly symmetric about the x axis. Similar to problem 1, the munitions sweep to the side to obtain differing viewpoints before closing in on the target.

The solution for the above initial conditions when applying the field-of-view constraint is listed as problem 4 in Table 1. The SLAP trajectories for this problem are shown in Fig. 4(b). The constraint is active for the early part of the trajectory of munition 1 and for the entire flight of munition 2.

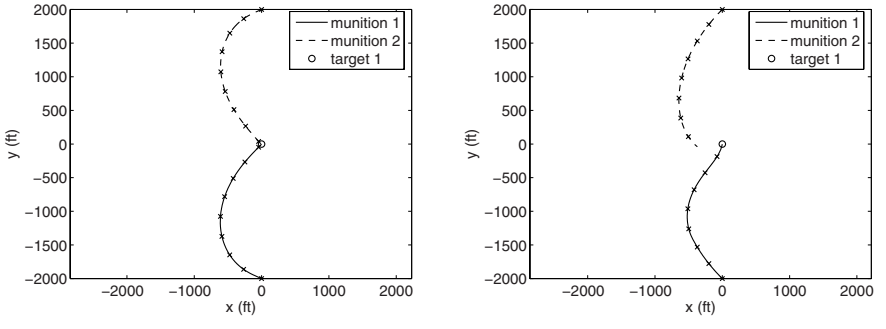

Fig. 4. SLAP trajectories for problems 3 and 4

5 Estimation Performance

The impact of the SLAP trajectories on the target-location estimation can now be evaluated. Although the trajectories were designed using a cost function based on the variances from a continuous WLSE algorithm, the estimation performance will be evaluated using a recursive weighted least squares estimation (RWLSE) algorithm with discrete measurement updates. First, the algorithm will be operated for a single munition following a trajectory from the initial condition straight to the target location (STT trajectory). Second, the estimation is performed for two munitions both following STT trajectories. Finally, the algorithm is implemented using two munitions following the field-of-view constrained SLAP trajectories. In each case, noisy measurements were simulated using the measurement model in Eq. (4).

The munition sensors were assumed to collect measurements of the target location at a rate of 10 Hz. The RWLSE algorithm operated as follows to determine the estimate and the uncertainty at the kth time step [21,22]. The current estimate is computed as follows.

$$\boldsymbol{K}_k = \boldsymbol{P}_{k-1}\boldsymbol{H}^\mathsf{T}\left(\boldsymbol{H}\boldsymbol{P}_{k-1}\boldsymbol{H}^\mathsf{T} + \boldsymbol{R}\right)^{-1} \tag{29}$$

$$\hat{\boldsymbol{x}}_k^{(T)} = \hat{\boldsymbol{x}}_{k-1}^{(T)} + \boldsymbol{K}_k\left(\tilde{\boldsymbol{z}}_k - \boldsymbol{H}\hat{\boldsymbol{x}}_{k-1}^{(T)}\right) \tag{30}$$

The current covariance matrix is computed as shown.

$$\boldsymbol{P}_k = \begin{bmatrix} \sigma_{x,k}^2 & \sigma_{xy,k} \\ \sigma_{xy,k} & \sigma_{y,k}^2 \end{bmatrix} = \left(\boldsymbol{P}_{k-1}^{-1} + \boldsymbol{H}_k^\mathsf{T}\boldsymbol{R}_k^{-1}\boldsymbol{H}_k\right)^{-1} \tag{31}$$

To compare the estimation performance along the different trajectories, the size of the one-sigma uncertainty ellipsoid in the target-location estimate can be used as a metric. At the kth time step, this is given by the product of π with the square root of the product of the eigenvalues of $\boldsymbol{P}_k$. In particular, the ellipsoid size at $t_F - 2\,\text{sec}$ will be highlighted. Although t_F is different for each trajectory, at this point in time munition 1 is roughly 600 ft from the target.

Using the initial condition of $x_1(0) = 0\,\text{ft}$, $y_1(0) = -2000\,\text{ft}$ the STT trajectory has a flight time given by $t_F = 6.67\,\text{sec}$. Using a single munition on an STT trajectory, at $t_F - 2\,\text{sec}$ the one-sigma uncertainty ellipse has an area of $81.5\,\text{ft}^2$. For $x_2(0) = 100\,\text{ft}$, and $y_2(0) = -2000\,\text{ft}$, adding measurements from munition 2 on an STT trajectory reduces the uncertainty to $39.7\,\text{ft}^2$. When the two munitions follow the SLAP trajectory shown in Fig. 3b, however, the area is reduced to $9.1\,\text{ft}^2$.

The error histories for a sample simulation with noisy measurements and three-sigma error bounds ($\pm 3\sigma_{x,k}$ and $\pm 3\sigma_{y,k}$) generated by the RWLSE algorithm are shown in Fig. 5. Figure 5(a) shows the errors in the x and y estimates of the target location using the STT trajectories. Figure 5(b) show the errors using the SLAP trajectories. Clearly, both trajectories give similar good performance in estimating the x component of the target location, but the SLAP trajectories provide much better estimation of the y component.

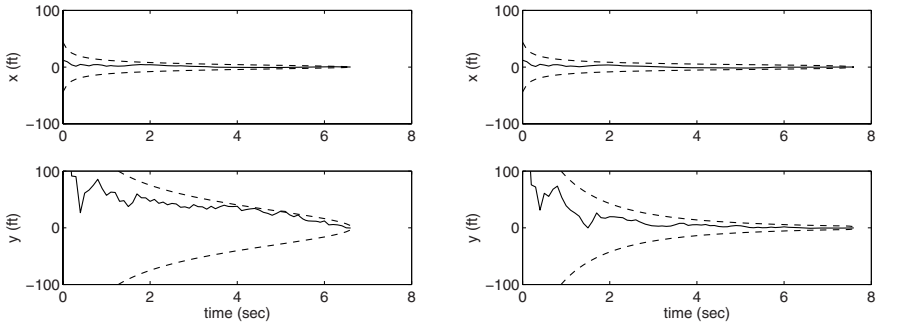

Fig. 5. Estimation errors using (a) STT and (b) SLAP trajectories with $x_2(0) = 100\,\text{ft}$, and $y_2(0) = -2000\,\text{ft}$

Moving munition 2 to the initial condition $x_2(0) = 0\,\text{ft}$, and $y_2(0) = 2000\,\text{ft}$ obviously does not change the results when only measurements from munition 1 are considered. For the cases with two munitions, however, the uncertainty areas at $t_F - 2\,\text{sec}$ are $40.8\,\text{ft}^2$ for the STT trajectories and $9.3\,\text{ft}^2$ for the SLAP trajectories. For these initial conditions, the error histories for a sample simulation with noisy measurements and three-sigma error bounds generated by the RWLSE algorithm are shown in Fig. 6.

These results give an indication of the impact of trajectory design on estimation performance. Significantly, for either initial condition, adding a second munition to help in the target-location estimation without paying attention to trajectory design improves performance to approximately half of the uncertainty achieved with a single munition. Careful use of the SLAP trajectories, however, further reduces the uncertainty to less than one quarter of what is achieved using

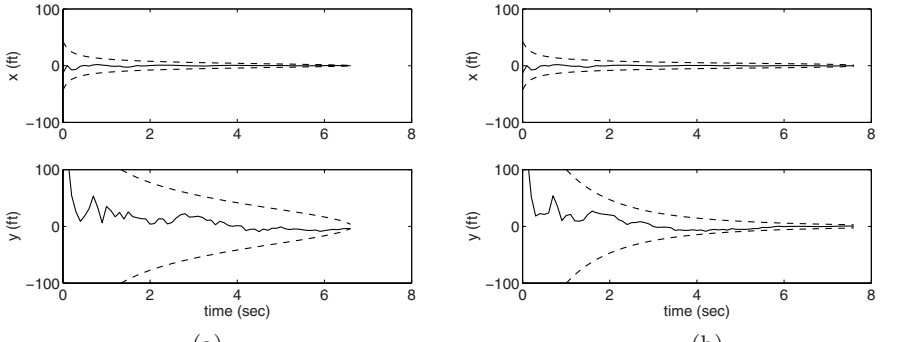

Fig. 6. Estimation errors using (a) STT and (b) SLAP trajectories with $x_2(0) = 0\,\text{ft}$, and $y_2(0) = 2000\,\text{ft}$

the STT trajectories. The SLAP trajectories benefit both from being delayed, which allows collection of more measurements, and their paths, which improve the quality of the measurements.

6 Conclusions

The results in the previous section demonstrate the impact that careful trajectory design can have on target-location estimation. Adding a second munition when following STT trajectories does significantly improve estimation performance. The use of the SLAP trajectories, however, reveals much greater further improvement. Furthermore, the complexity and cost of the second munition and communication between the two has already been accepted in taking the first step. The second step of following the SLAP trajectories only requires careful trajectory design.

Improvements in estimation performance like those demonstrated here could have significant impact on munition design and cost. More accurate target-location estimation could allow more accurate strike capability or the ability to attack targets that are difficult to detect. It is anticipated that the reduction in uncertainty early in the trajectory could be critical for the precision strike of these difficult targets; however, further work is needed to demonstrate the impact of these estimation enhancements on guidance and control performance. Combined, these effects could enable the use of smaller, cheaper munitions against targets in cluttered environments while limiting collateral damage.

The calculus-of-variations approach, used here, to solve for SLAP trajectories allowed for model-based trajectory design. This approach may not be the best approach, however, for real-time implementation. Future work for this application may require different solution approaches. The intuition gained from calculus-of-variations based sample solutions may allow the development of heuristic solutions that are better suited for real-time implementation.

References

1. Chandler, P.R., Pachter, M., Nygard, K.E., Swaroop, D.: Cooperative control for target classification. In Murphey, R., Pardalos, P.M., eds.: Cooperative Control and Optimization, Kluwer, Netherlands (2002) 1–19
2. Jeffcoat, D.E.: Coupled detection rates: An introduction. In Grundel, D., Murphey, R., Pardalos, P.M., eds.: Theory and Algorithms for Cooperative Systems, World Scientific, New Jersey (2004) 157–167
3. Frew, E., Lawrence, D.: Cooperative stand-off tracking of moving targets by a team of autonomous aircraft. In: AIAA Guidance, Navigation, and Control Conference, San Fancisco, California (2005) AIAA-2005-6363.
4. Fawcett, J.A.: Effect of course maneuvers on bearings-only range estimation. IEEE Transactions on Acoustics, Speech, and Signal Processing **36** (1988) 1193–1199
5. Hammel, S.E., Liu, P.T., Hilliard, E.J., Gong, K.F.: Optimal observor motion for localization with bearing measurements. Computers and Mathematics with Applications **18** (1989) 171–180

6. Logothetis, A., Isaksson, A., Evans, R.J.: Comparison of suboptimal strategies for optimal own-ship maneuvers in bearings-only tracking. In: American Control Conference, Phiadelphia, Pennsylvania (1998)
7. Passerieux, J.M., VanCappel, D.: Optimal observer maneuver for bearings-only tracking. IEEE Transactions on Aerospace and Electronic Systems **34** (1998) 777–788
8. Oshman, Y., Davidson, P.: Optimization of observer trajectories for bearings-only target localization. IEEE Transactions on Aerospace and Electronic Systems **35** (1999) 892–902
9. Frew, E.W., Rock, S.M.: Trajectory generation for constant velocity target motion estimation using monocular vision. In: IEEE International Conference on Robotics & Automation, Taipei, Taiwan (2003)
10. Watanabe, Y., Johnson, E.N., Calise, A.J.: Vision-based guidance design from sensor trajectory optimization. In: AIAA Guidance, Navigation, and Control Conference, Keystone, Colorado (2006) AIAA-2006-6607.
11. Grocholsky, B.: Information-Theoretic Control of Multiple Sensor Platforms. PhD thesis, University of Sydney, Sydney, Australia (2002)
12. Ousingsawat, J., Campbell, M.E.: Optimal cooperative reconnaissance using multiple vehicles. Journal of Guidance, Control, and Dynamics **30** (2007) 122–132
13. Dohner, J.L., Eisler, G.R., Driessen, B.J., Hurtado, J.: Cooperative control of vehicle swarms for acoustic target localization by energy flows. Journal of Dynamic Systems, Measurement, and Control **126** (2004) 891–895
14. Passino, K., Polycarpou, M., Jacques, D., Pachter, M., Liu, Y., Yang, Y., Flint, M., Baum, M.: Cooperative control for autonomous air vehicles. In Murphey, R., Pardalos, P.M., eds.: Cooperative Control and Optimization, Kluwer, Netherlands (2002) 233–271
15. Pachter, M., Hebert, J.: Cooperative aircraft control for minimum radar exposure. In Murphey, R., Pardalos, P.M., eds.: Cooperative Control and Optimization, Kluwer, Netherlands (2002) 199–211
16. Zabarankin, M., Uryasev, S., Pardalos, P.: Optimal risk path algorithms. In Murphey, R., Pardalos, P.M., eds.: Cooperative Control and Optimization, Kluwer, Netherlands (2002) 273–303
17. Murphey, R., Uryasev, S., Zabarankin, M.: Optimal path planning in a threat environment. In Butenko, S., Murphey, R., Pardalos, P., eds.: Recent Developments in Cooperative Control and Optimization, Kluwer, Netherlands (2004) 349–406
18. Kabamba, P.T., Meerkov, S.M., III, F.H.Z.: Optimal path planning for unmanned combat aerial vehicles to defeat radar tracking. Journal of Guidance, Control, and Dynamics **29** (2006) 279–288
19. Pachter, M., Chandler, P.R., Purvis, K.B., Waun, S.D., Larson, R.A.: Multiple radar phantom tracks from cooperating vehicles using range-delay deception. In Grundel, D., Murphey, R., Pardalos, P.M., eds.: Theory and Algorithms for Cooperative Systems, World Scientific, Singapore (2004) 367–390
20. Purvis, K.B., Chandler, P.R., Pachter, M.: Feasible flight paths for cooperative generation of a phantom radar track. Journal of Guidance, Control, and Dynamics **29** (2006) 653–661
21. Stengel, R.F.: Optimal Control and Estimation. Dover, New York (1986)
22. Crassidis, J.L., Junkins, J.L.: Optimal Estimation of Dynamic Systems. Chapman & Hall/CRC, Boca Raton, Florida (2004)
23. Bryson, A.E., Ho, Y.C.: Applied Optimal Control: Optimization, Estimation, and Control. Hemisphere Publishing Corporation, Washington, District of Columbia (1975)